6th European Conference on Computational Mechanics (ECCM 6)
7th European Conference on Computational Fluid Dynamics (ECFD 7)
1115 June 2018, Glasgow, UK

FORCES ON A SUBMERGED SUB SEA TIDAL KITE IN SURFACE PROXIMITY

Pál Schmitt[1], Daniel Ferreira González[2], Ulf Göttsche[2], Christian W. Schulz[2], Stefan Netzband[2], Martin Scharf[2], Moustafa Abdel-Maksoud[2] and Louise Kregting[1]

[1] Marine Research Group, Queen's University Belfast, BT11 1PF Portaferry, Northern Ireland

[2] Institute for Fluid Dynamics and Ship Theory, Technische Universität Hamburg, Hamburg, Germany

Key words: tidal energy, hydrofoil, Boundary Element Method (BEM), *pan*MARE, marine renewable, wave current interaction

Abstract. Sub-sea tidal kites, while still at an early stage of development, might be an efficient and cost effective way of extracting energy from marine currents [9]. During normal operating conditions the kite is positioned deep in the water column and would ideally be built neutrally buoyant. For operation and maintenance (O&M) situations, or if a fault occurs, it is important to surface the kite in a controlled manner. While the behaviour of wing like profiles in currents is well understood, the assessment of the behaviour in surface proximity and under wave action is not trivial [1].

We employ an efficient boundary element code called *pan*MARE [2] to simulate the effect of surface proximity and wave current interaction on a sub-sea kite. Comparison with experimental data from [1] demonstrates the suitability of the method to simulate forces on a submerged foil for varying immersion depths and angles of attack. Simulations are then performed to investigate the combined effect of waves and current to inform on the most suitable met-ocean conditions for kite retrieval.

1 INTRODUCTION

The sub-sea kite system which inspired the work presented in this paper is being developed by the company Minesto AB [9, 3, 8]. The kite consists of a fixed wing, under which a nacelle is attached. Figure 1 shows a quarter scale prototype being launched. Rudders and elevators at the end of the nacelle allow the kite flight path to be controlled. A turbine is located at the front of the nacelle, facing the undisturbed inflow. A tether is connected via a two point link to the left and right side of the wing and an adjustable strut connects to the rear of the nacelle. By adjusting the length of this rear-strut the angle of attack of the wing can be controlled during operation. The kite is flown in figures of eight, accelerating to velocities up to 10 times the ambient flow. The high relative velocity drives the turbine, which is connected to an electric generator. Electricity

Figure 1: Quarter scale kite during testing

and communication signals are transported through the tether. During normal operating conditions, a neutrally buoyant kite would be ideal. However, for maintenance, installation and retrieval the kite must be brought to the surface in order to be connected to a vessel or lifted out of the water by a crane and thus the hydrodynamics close to the surface become important. The kite with its optimised hydrodynamic shape experiences considerable load variations even for small changes in inflow velocity and direction. Some aspects of the hydrodynamics of hydrofoils in surface proximity have been investigated in detail. The main focus has been on the loss of lift when a hydrofoil approaches surface proximity. This paper presents an initial investigation on the effect of surface proximity and the interaction of wave and current loading on a kite using the boundary element method. The numerical tool used is *pan*MARE [2]. The paper is structured in four sections. Section 1 presents an overview on the numerical methods. Section 2 presents results of a validation study against experimental and other numerical data for a hydrofoil under current conditions for different depths. The third section present initial results on the the influence of waves and current on a hydrofoil with similar dimensions as the full-scale kite system followed by the conclusions.

2 NUMERICAL APPROACH

The program *pan*MARE is a boundary element method based on potential theory, see [4, 5]. The basic code follows the theory published in [6]. Here, Φ is the total potential of the fluid with the spatial derivative $\nabla\Phi$ which is the fluid velocity. As the fluid is assumed to be inviscous, irrotational and incompressible the conservation equation can be simplified to the Laplace equation:

$$\Delta\Phi = \nabla^2\Phi = 0\,. \tag{1}$$

Due to the linearity the total potential can be divided into two parts:

$$\Phi = \phi_i + \phi_e\,, \tag{2}$$

where ϕ_i denotes the induced potential and ϕ_e defines an external potential. In the present work the waves are included as external potential into the simulation. Following Airy theory, the potential of a wave, defined by amplitude ζ_a, frequency ω and phase information ϵ, at a certain position $\mathbf{x}$ and time t is:

$$\phi_e(\mathbf{x},t) = -\zeta_a \frac{\omega}{k} \frac{\cosh\left(k\left(z+d\right)\right)}{\sinh\left(k\,d\right)} \mathrm{Re}\left\{ i\, e^{i\,\left(-\omega t + k\; x + \epsilon\right)} \right\}. \tag{3}$$

Here, k is the wave number and d is the water depth.

The surface of the body S_b and of the free water surface S_{fs} is discretized by panels. Each panel has a constant source σ and dipole μ distribution, thus, the induced potential can be described as

$$\phi_i = \frac{1}{4\pi} \int_S \left[\mu \frac{\partial}{\partial\, n} \frac{1}{r} - \sigma \frac{1}{r} \right] \mathrm{d}S\,. \tag{4}$$

The source strength of the body panels is computed applying the Neumann boundary condition:

$$\nabla\Phi - \mathbf{v}_m = 0\,, \tag{5}$$

where $\mathbf{v}_m$ is the velocity of the panel. Then, the unknown doublet strength μ_b on the body surface can be determined by employing the Dirichlet boundary condition

$$\Phi\left(\mathbf{x},t\right) = \phi_e\,, \quad \text{for} \quad \mathbf{x} \notin \mathcal{V}\,, \tag{6}$$

, which ensures that the induced potential ϕ_i is zero outside the volume $\mathcal{V}$ at each instant of time t, by solving the resulting linear equation system (LES). The Mixed-Eulerian-Langriangian (MEL) method [7] is used to include the free water surface. It consists of two steps. In the first one, the source strengths σ_{fs} of the free surface panels are solved within the LES employing the Dirichlet boundary condition. Then, in the second step, the time derivatives $\partial\zeta/\partial t$ and $\partial\phi_i/\partial t$, which follow from the kinematic and dynamic free surface condition, are integrated. This yields elevation ζ and induced potential ϕ_i at the free water surface which are taken over to the next time step. Due to the fact that viscosity is not being accounted for in potential methods like *pan*MARE, the simulated flow would stay attached to the body even under strongly adverse pressure gradients, for example at the body trailing edge. To model the physical detachment at this part of lifting bodies, an infinitely thin material surface is introduced starting at the trailing edge. This surface is generally referred to as the wake and represents the vorticity shed by the body in realistic flows. Enforcing a no-flow condition through this surface the kinematic boundary condition requires a deformation of this surface based on the flow velocity. Additionally, the dynamic boundary condition specifies equal pressure at both sides of this surface, hence also at the trailing edge. The latter is satisfied with one additional unknown singularity for each discretized trailing edge segment and timestep. It is usually solved in the linear Morino Kutta form directly for the wake doublet strength

$$\mu_w = \mu_{upper} - \mu_{lower} \tag{7}$$

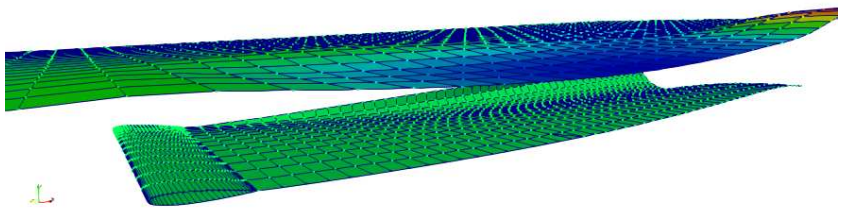

Figure 2: Surface Elevation and wake for h/c=4.

which is then substituted in the equations using the doublet strengths at the upper side μ_{upper} and lower side μ_{lower} of the body at the trailing edge. For flows that leave the trailing nearly perpendicularily this is a sufficiently accurate linearization. In more complicated cases the iterative nonlinear Kutta condition can be applied instead.

3 VALIDATION FOR HYDROFOILS

[1] presented a study investigating the the changes in lift depending on depth for a hydrofoil. Experiments were performed for a hydrofoil with a wingspan of 0.924 m and a chord length of 0.111 m. The flow velocity was 3 m/s. Simulations were run reproducing those test cases for an angle of attack of seven and eight degrees. Depth d is normalised by dividing by the chord length c. Although not presented here in detail, first studies were run to investigate the effect of the size of the computational domain, suitable resolution of the surface, wing and wake panels. Results were found to show little variation around the following settings which were then used in the actual study. The domain was discretisation on the surface with 60 times 40 grid cells. The hydrofoil, a NACA 0012 profile was discretised with a panel distribution of 30 panels over the chord length as shown in Figure 2.

Figure 3 presents an initial study reproducing the coefficient of lift C_L on the y-axis over the angle of attack. Results are given for the analytical solution, current *pan*MARE results and the experimental data as given by [1]. Up to an angle of attack of 5° agreement between all three methods is good. For larger angles of attack the experimental results are considerably higher than the analytical solution while *pan*MARE results are somewhat lower. While the *pan*MARE results follow a linear trend, increasing over the angle of attack as would have been expected from the analytical solution, the experimental data shows an offset between 4° and 6°. The reasons for these discrepancies are unclear.

Figure 4 shows results for an angle of attack of 7°. The top half shows surface elevation for a normalised depth of one, in the lower half the surface elevation can be seen for a normalised depth of four. The characteristic wave pattern, consisting of a trough followed by a smaller wave crest, can clearly be seen. The change in surface elevation is orders of magnitude larger for the first case when compared to the second.

Figure 5 presents the coefficient of lift normalised with the lift value at maximum depth over normalised depth for an angle of attack of 7° (left) and 8° (right). Experimental data is presented with *pan*MARE results and earlier analytical solutions from Wadlin and

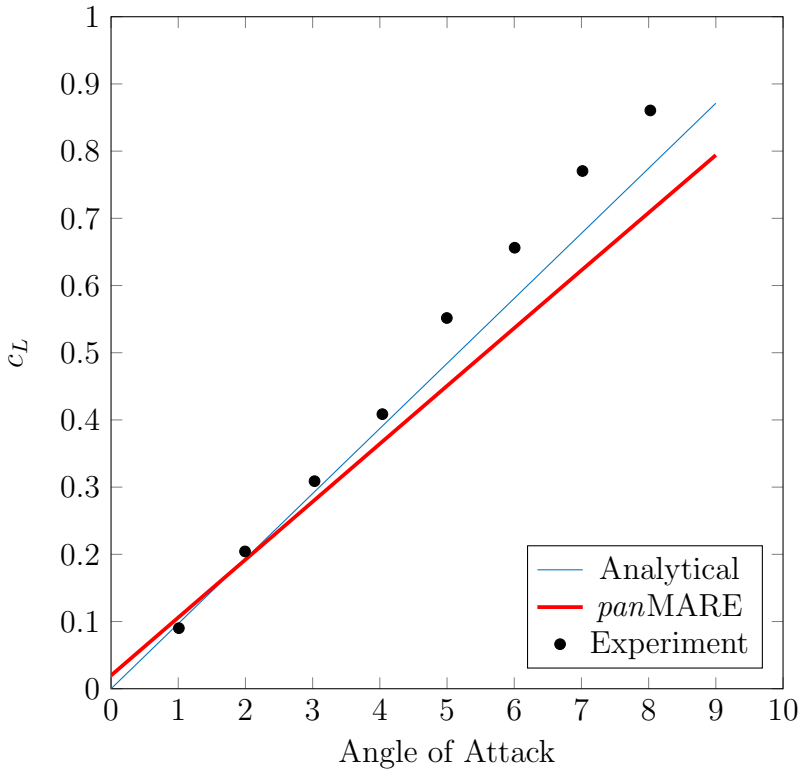

Figure 3: Lift coefficient over angle of attack as obtained from experimental measurements, analytical models and present simulations.

Payne. The experimental data shows some nonphysical properties, but the overall trend of decreasing lift with decreasing depth is well captured. The *pan*MARE results show those changes and for larger depth values agree well with the experimental data and the method presented by Wadlin. For a normalised depth between zero and two the current *pan*MARE results match the experimental results better than the results of Wadlin.

For an angle of attack of 8° agreement between experimental data and *pan*MARE is better than between experimental data and the Wadlin method. Considering the scatter and clearly un-physical features of the experimental results, *pan*MARE results reproduce the physics well.

4 KITE CASES

Simulations were then run for hydrofoil representing the sub-sea kite with a wingspan of 12 m and a chord length of 2 m. The flow velocity is one metres per second and the wave height was set to 0.5 m and a period of 3 s. As a baseline case simulations were run for a wave travelling with the current direction, that is an encounter angle of 0°. Figure 6 shows the surface elevation seen from the top on the left and to the right the kite with the wake developing behind it seen from below. As a comparison, results for waves running in the opposite direction of the current are shown in Figure 7. The effect of the waves on the wake can clearly be seen in this case. For an encounter angle of 0° the wake shows an

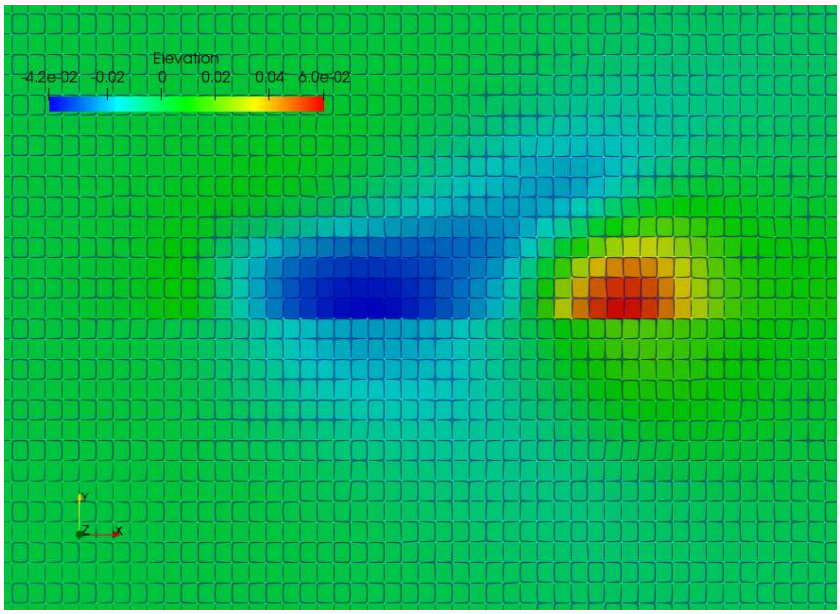

Figure 4: Surface Elevation for h/c=1 (top) and h/c=4 (bottom)

oscillatory motion following the wave. Higher frequency oscillations of the wake can be observed when the waves run against the current.

Another case of practical interest is waves incoming at different angles. Figure 8, 9 and 10 show waves at an encounter angle of 45, 90 and 135°. It can clearly be observed how the wake is distorted and bending in wave direction. Interestingly, in most of those cases the wake is not shed in a regular pattern.

Figure 11 presents the vertical force on the kite over the simulation time of 20 seconds. With the current settings it takes 10 seconds for the wake to fully develop and in some cases, for example for the 90° encounter angle, it can be seen that a regular motion only develops after that time. Similarly findings apply to the case of 45 and 0 degree. For the case of 180° and 135° no regular force variation is reached. For the three cases which settle into a regular oscillating force the amplitude decreases with increasing encounter angle. Overall, the 90° case shows smallest force amplitude variations.

A second series of tests was run for a five second wave period and varying depths. The wave field and the wake deformation for a depth of 1.5 m and a depth of 4 m is shown in Figures 12 and 13. Figure 14 shows the resulting horizontal force component over time. Even after 20 s it is not clear whether a steady-state solution has been reached. Over time the force amplitudes increase, indicating some transient effect. Differences in force variations are always larger during the peak then in the trough. However, results do indicate as expected that the wave induced forces and wake motions decreases considerably with increasing depth.

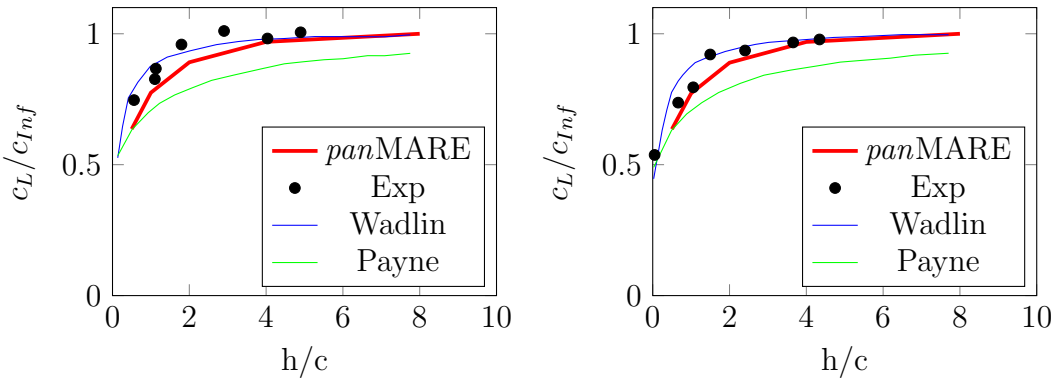

Figure 5: Normalised lift over normalised depth for AoA 7*deg* (left) and 8*deg* (right)

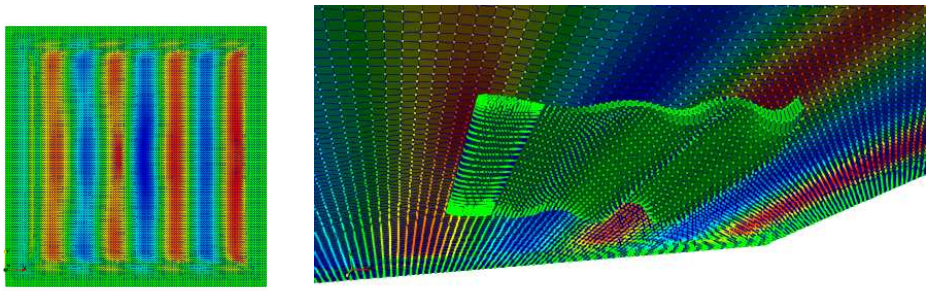

Figure 6: Wakedeformation. Dir 0

5 CONCLUSIONS

This paper presented first simulations of a sub-sea kite in surface proximity. Validation runs show that *pan*MARE is a suitable tool for such investigations, yielding good results with orders of magnitude less computational demand than RANS CFD tools.

Initial results for the full-scale kite indicate that horizontal loading on a kite in surface proximity will decrease with an encounter angle closer to 90°. However, we have not evaluated the resulting torque moment which will of course cause a rolling motion of the kite. Further simulations are required to understand why the horizontal force traces do not converge for angles larger than 90°. The study also highlights the need for accurate experimental data to validate numerical tools. *pan*MARE can be used in the future to simulate a kite even with time varying angles of attack as might be provided by a control system and resulting motions in surface proximity.

6 AKNOWLEDGEMENTS

This project has received funding from the European Union's Horizon 2020 research and innovation programme under grant agreement No 654438.

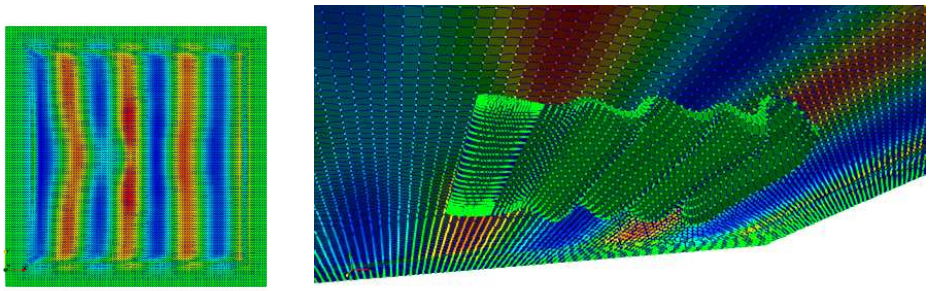

Figure 7: Wakedeformation. Dir 180

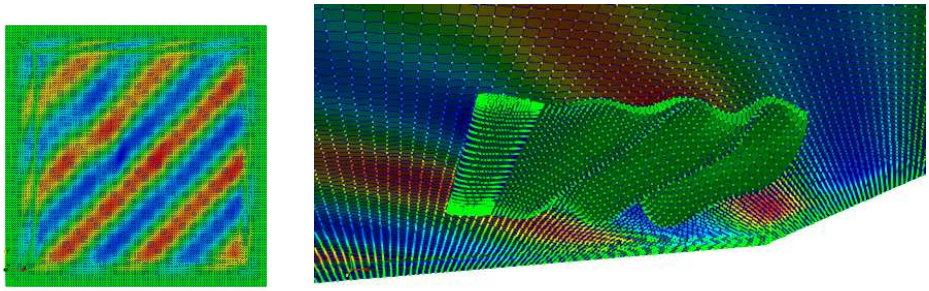

Figure 8: Wakedeformation. Dir 45

REFERENCES

[1] M. Daskovsky. The hydrofoil in surface proximity, theory and experiment. *Ocean Engineering*, 27(10):1129–1159, 2000. cited By 6.

[2] D. Ferreira González, J. Bechthold, and M. Abdel-Maksoud. Application of a boundary element method for wave-body interaction problems considering the non-linear water surface. volume 7A-2017, 2017. cited By 1.

[3] S. T. Fredriksson, G. Broström, M. Jansson, H. Nilsson, and B. Bergqvist. Large eddy simulation of the tidal power plant deep green using the actuator line method. *IOP Conference Series: Materials Science and Engineering*, 276(1):012014, 2017.

[4] M. Gaschler. *Numerical Modelling and Simulation of Cavitating Marine Propeller Flows*. PhD thesis, Institute for Fluid Dynamics and Ship Theory, 2017.

[5] M. Greve. *Non-viscous calculation of propeller forces under consideration of free surface effects*. PhD thesis, Hamburg University of Technology, 2015.

[6] Joseph Katz and Allen Plotkin. *Low-Speed Aerodynamics*. Number 13 in Cambridge Aerospace Series. Cambridge University Press, 2nd edition, 2001.

[7] Michael S. Longuet-Higgins and E.D. Cokelet. The deformation of steep surface waves on water. I. A numerical method of computation. In *Proceedings of the Royal Society*

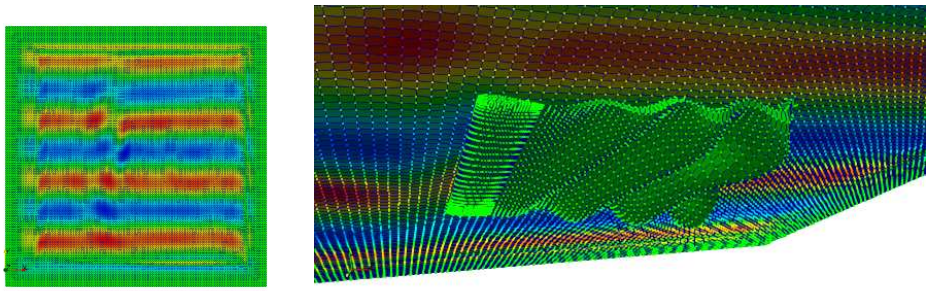

Figure 9: Wakedeformation. Dir 90

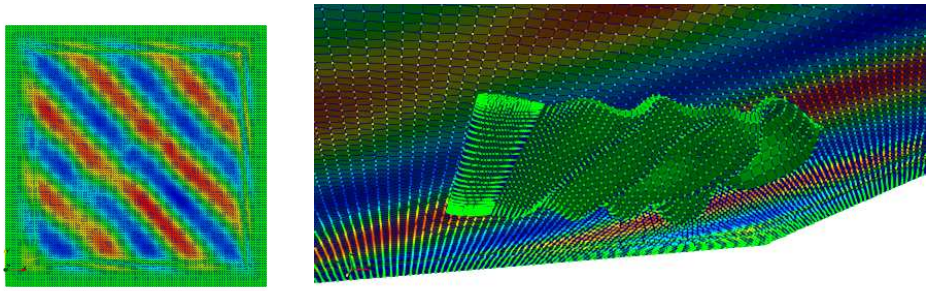

Figure 10: Wakedeformation. Dir 135

of London A: Mathematical, Physical and Engineering Sciences, volume 350, pages 1–26. The Royal Society, 1976.

[8] P. Schmitt, R. Culloch, L. Lieber, S. Molander, L. Hammar, and L. Kregting. A tool for simulating collision probabilities of animals with marine renewable energy devices. *PLOS ONE*, 12(11):1–11, 11 2017.

[9] C. Zambrano. Lessons learned from subsea tidal kite quarter scale ocean trials. In *WTE16 - Second Workshop on Wave and Tidal Energy*, Valdivia, Chile, November 2016.

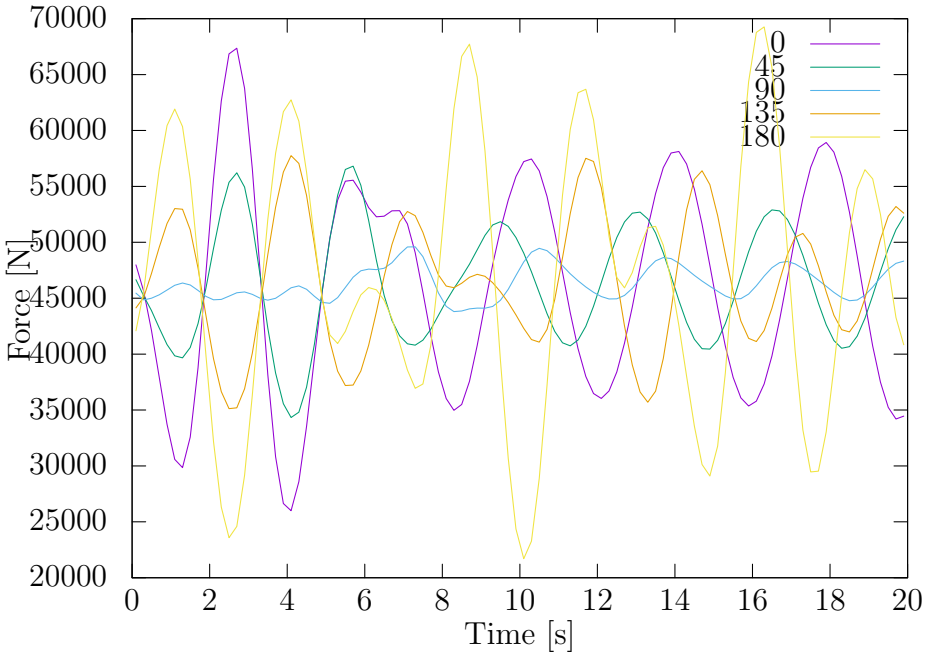

Figure 11: Vertical Force over time for wave direction varying from 0 to 180, Depth 2m.

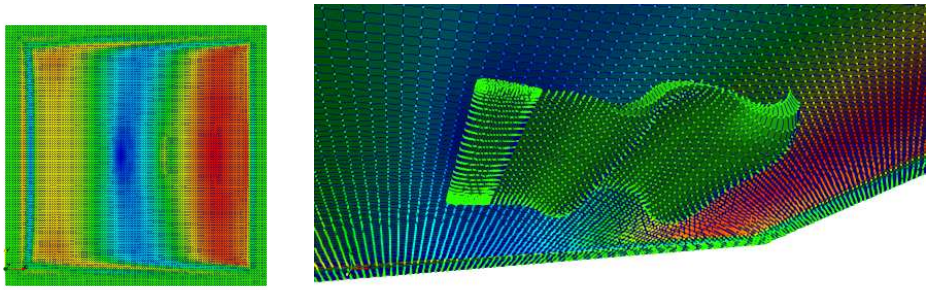

Figure 12: Wakedeformation. D 1.5m

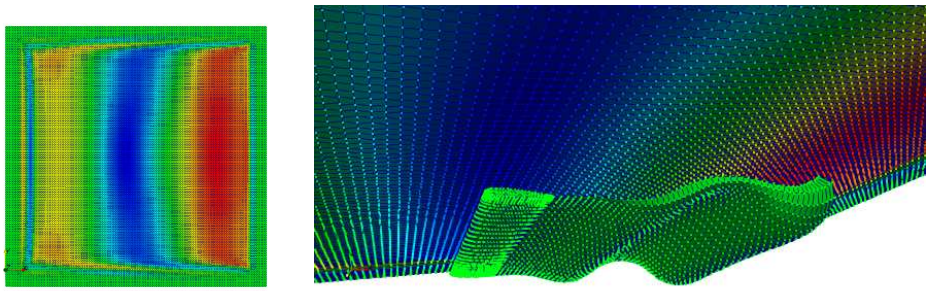

Figure 13: Wakedeformation. D 4m

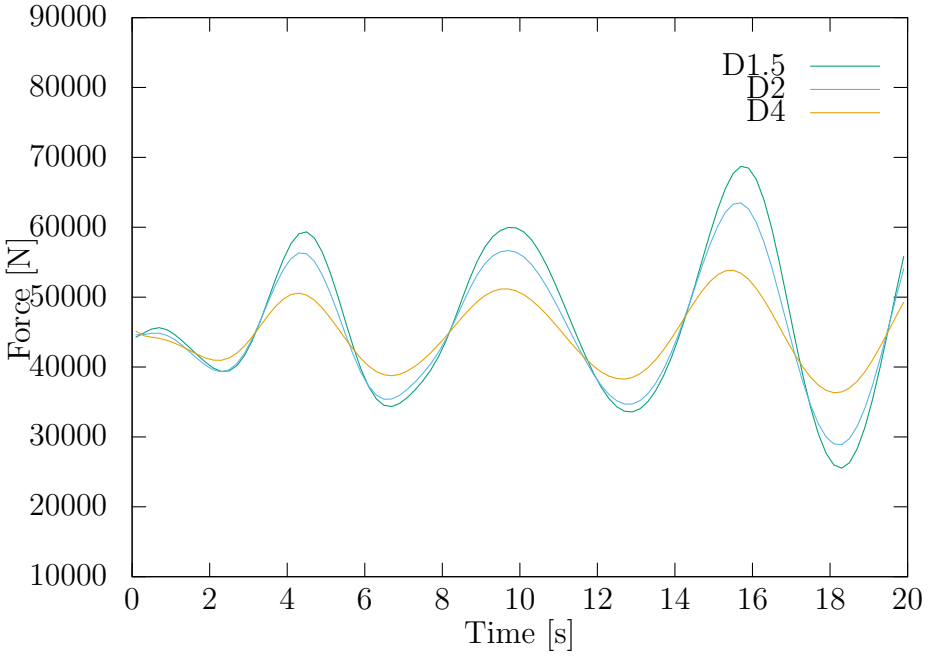

Figure 14: Vertical Force over time, Depth varying from 1-4m, Waveangle 0.